Kaon photoproduction from nuclei in a relativistic nuclear model

C. Bennhold* and L. E. Wright
Department of Physics and Astronomy, Ohio University, Athens, Ohio 45701
(Received 26 September 1988)

The formation of hypernuclei through the photoproduction of kaons is formulated in the framework of a relativistic distorted wave impulse approximation. The basic production operator is based on diagrammatic techniques and includes low-lying baryon and meson resonances. Relativistic single-particle wave functions obtained by solving the Dirac equation with scalar and timelike vector potentials are employed to describe the nucleon and hyperon bound states. The nuclear and hypernuclear structure is described in a pure single-particle single-hole model. Evaluating the matrix elements in momentum space allows straightforward treatment of Fermi motion and naturally includes nonlocalities arising from the production operator. Different nonrelativistic limits involving the upper and lower component of the Dirac wave function and a p/M expansion of the operator are investigated. The final-state interaction of the weakly absorbed kaon is incorporated via an optical potential. A variety of angular distributions for p-shell nuclei is presented and the sensitivity of the hypernuclear cross sections to the elementary operator is shown to be important. Relativistic effects are found to be important along with effects of nonlocalities for low-spin states while high-spin states with large cross sections are less affected. Kaon distortion for p-shell nuclei only provides a slight reduction in cross section for most transitions.

I. INTRODUCTION

The study of hypernuclei is becoming one of the important new fields in nuclear physics.[1-5] This is due to a number of theoretical and experimental improvements in recent years as well as the growing awareness of the importance of quark and meson degrees of freedom in the nucleus. If we assume the nucleus to be a system of nucleons and mesons, rather than quarks, it is possible to implant a lambda into a nucleus in any state that is energetically possible, including the lowest s state, since the lambda is not blocked by the Pauli principle. As the lifetime of the lambda is long enough to form a stable system, a whole new regime of nuclear structure studies from the lightest systems throughout the periodic table is opening up.

This investigation focuses on the formation of lambda hypernuclear states through the photoproduction of charged kaons. With continuous beam electron linacs on the horizon with sufficient energy and intensity, this reaction is attracting a great deal of attention.[6-9] Since it preferentially excites unnatural parity and high-spin states, it complements the reactions (K^-,π^-) and (π^+,K^+) which selectively excite natural parity states and from which most of the information on hypernuclei has been extracted until now.[10,11]

The (K^-,π^-) reaction has the advantage that the mass of the incoming K^- is much larger than the mass of the outgoing π^-, thus allowing the production of the lambda with low or zero momentum transfer to the residual nucleus. As a consequence, counting rates are high, but low momentum transfer does limit the spectrum of excited states mainly to substitutional and low-spin transitions. Kaon photoproduction shares its spin and momentum transfer capabilities with the second, purely hadronic, reaction (π^+,K^+) that has been used to produce hypernuclei. Due to the large production of rest mass in these two reactions, the momentum transfer to the residual nucleus becomes sizable and, therefore, these reactions will project out high momentum components of the nuclear wave functions. Since high angular momentum form factors tend to peak at larger Q values, high-spin states are preferentially excited. However, (γ,K^+) excites both spin-flip and non-spin-flip transitions while (π^+,K^+) primarily leads to non-spin-flip transitions so that these two reactions are complementary.

An advantage with photoproduction is that both the photon and the K^+, with its mean free path of about 5–7 fm in the nuclear medium, interact rather weakly with the nucleus so that the process can occur deep in the nuclear interior as compared to K^- and $\pi^\pm$ which are both strongly absorbed, thereby confining the reaction to the nuclear periphery. This penetrating property of the photon and the K^+, together with a reasonably well understood production mechanism, offer a unique opportunity to study, in a "clean" way, nuclear and hypernuclear wave functions and structure effects.

In the current work we consider the $A(\gamma,K^+)_\Lambda B$ reaction in a relativistic impulse approximation framework.[12] That is, the incoming photon interacts with a bound nucleon (proton) creating a lambda which goes into a bound state and a K^+ which exits the nucleus. This production process in the nuclear medium is assumed to be given by the free process $p(\gamma,K^+)\Lambda$ which is described by first-order Feynman diagrams. We use a representation of this reaction which includes the Born terms in addition to low-lying nucleon, meson, and hyperon resonances for which the coupling constants have been fitted to photoproduction data up to 1.4 GeV.[13,14] The distortion of the outgoing kaon is included via a rather weak optical

potential, which has been derived from the elementary KN amplitudes. This approach to kaon photoproduction from nuclei seems reasonable following the success of a similar treatment of pion photoproduction from p-shell nuclei,[15] and the recent (π^+,K^+) results from Brookhaven[11] which find evidence of single-particle Λ orbits for a range of nuclei up to $^{89}_{\Lambda}$Y.

The single-particle bound-state wave functions are taken to be solutions of the time-independent Dirac equation with real scalar and timelike vector potentials which represent a local Lorentz covariant interaction of the single nucleon or lambda with the remaining $(A-1)$ nucleons. The Dirac approach, giving credence to relativistic nuclear dynamics, not only provides improved descriptions of proton-nucleus elastic scattering,[16] but is able to naturally explain the spin-orbit splitting in the nuclear shell model.[17] Calculations involving Dirac-Hartree and Dirac-Hartree-Fock methods have been performed[18] and provide nuclear densities in good agreement with electron scattering data. Since the scalar and vector potentials are of the order of the nucleon mass and the kaon photoproduction reaction requires large three-momentum transfer to the nucleus, the conventional reduction of the free production operator to an effective nonrelativistic nuclear operator may omit important effects.[19] Following the work of Tiator and Wright on pion photoproduction,[15] the analysis is carried out in momentum space, rather than in coordinate space, in order to straightforwardly include all the nonlocalities in the production operator arising from the propagation of various baryons and mesons. In other theoretical work,[6,7,9] nonlocal effects have been ignored by using the frozen nucleon approximation in the production operator or in more recent work[8] have been included in an approximate way. Since no data are as yet available for kaon photoproduction from nuclei, rough estimates of expected counting rates, neglecting nonlocalities or including them in an approximate way was certainly justified. However, previous work on pion photoproduction has shown that complete neglect of nonlocalities is not a good approximation except for special cases, and in some cases they need to be included quite precisely.

In Sec. II we discuss our parameters for the Dirac and Schrödinger equations, and in Sec. III we briefly describe the kaon optical potential. The general formalism for calculating relativistic matrix elements in momentum space is presented in Sec. IV. In Sec. V we examine nonrelativistic reductions concerning the nature of the small and large component of the Dirac wave function and the reduction of the operator itself. Commonly used plane wave and local approximations are introduced in Sec. VI. We apply our formalism to various reactions in the p shell in Sec. VII and present angular distributions for a variety of beam energies to document significance of relativistic effects, nonlocalities and kaon distortion. Finally, we summarize our findings in Sec. VIII.

II. DIRAC AND SCHRÖDINGER BOUND STATE WAVE FUNCTIONS

To obtain relativistic single-particle wave functions we solve the time-independent Dirac equation

$$[p-m-S(r)-\gamma^0 V(r)]\psi^{\mu}_{n\kappa}(\mathbf{r})=0\ , \tag{1}$$

where $S(r)$ and $V(r)$ are real scalar and timelike vector potentials that can be thought of as generated by σ and ω exchange in the mean-field approximation.[20] The solution to Eq. (1) can be written as

$$\psi^{\mu}_{n\kappa}(\mathbf{r})=\begin{bmatrix} f_{n\kappa}(r)\chi^{\mu}_{\kappa}(\hat{\mathbf{r}},s) \\ ig_{n\kappa}(r)\chi^{\mu}_{-\kappa}(\hat{\mathbf{r}},s)\end{bmatrix}\ , \tag{2}$$

where the spin-angle functions χ^{μ}_{κ} are given by

$$\chi^{\mu}_{\kappa}(\hat{\mathbf{r}},s)=\sum_{m_s,m_l} C^{l(1/2)j}_{m_l m_s \mu} Y^{m_l}_{l}(\hat{\mathbf{r}})\xi^{m_s}_{1/2} \tag{3}$$

and the angular momentum labels j and l are given in terms of the Dirac quantum number κ by $j=|\kappa|-\frac{1}{2}$ and $l=|\kappa+\frac{1}{2}|-\frac{1}{2}$. The label n is the usual quantum number counting the radial nodes.

Usually nonrelativistic shell model analyses make use of a harmonic oscillator potential without a spin-orbit term, and, therefore, the wave functions are only characterized by a range parameter b even though a potential with a Woods-Saxon shape

$$h(r)=\frac{1}{1+\exp\left[\dfrac{r-R}{a}\right]}\ , \tag{4}$$

where $R=r_0 A^{1/3}$ and a are the radius and diffuseness parameters is known to furnish a better description for high momentum transfer processes. To generate realistic nonrelativistic wave functions we insert a central and spin-orbit potential of the following form into the Schrödinger equation:

$$V(r)=V_{\rm cen}h(r)+\frac{V_{\rm so}}{m_\pi^2}\boldsymbol{l}\cdot\mathbf{S}\frac{1}{r}\frac{dh}{dr}\ . \tag{5}$$

The potentials $S(r)$ and $V(r)$ in the Dirac equation are also written in terms of the Woods-Saxon shape $h(r)$ with strengths S_0 and V_0, which are of order 400 MeV, but of opposite sign ($S_0<0, V_0>0$). The depths of the relativistic potentials S_0 and V_0, as well as the central and spin-orbit potentials $V_{\rm cen}$ and $V_{\rm so}$ were adjusted to fit s- and p-shell binding energies and spin-orbit splittings, while the geometry parameters were chosen for each case to yield the correct rms radius. Note that the geometry parameters differ for the Schrödinger and Dirac potentials, but we did constrain the scalar and vector potential to have the same radius and diffuseness parameters. As an example, Table I gives the parameters for the $A=16$ sys-

TABLE I. Potential depths (MeV) and geometry parameters (fm) for the $A=16$ system.

		Dirac		
Proton	$S_0=-395$	$V_0=295$	$r_0=0.9$	$a=0.7$
Lambda	$S_0=-116$	$V_0=84$	$r_0=1.1$	$a=0.7$
		Schrödinger		
Proton	$V_{\rm cen}=60$	$V_{\rm so}=16$	$r_0=1.2$	$a=0.6$
Lambda	$V_{\rm cen}=28$	$V_{\rm so}=1$	$r_0=1.2$	$a=0.6$

TABLE II. Single-particle s- and p-shell separation energies for the lambda and the proton in $^{16}_{\Lambda}$N and ^{16}O (in MeV).

	State	Dirac	Schrödinger	Experiment
Proton	$0s_{1/2}$	−43.6	−33.2	−44
	$0p_{3/2}$	−17.8	−18.4	−18.4
	$0p_{1/2}$	−12.1	−12.9	−12.1
Lambda	$0s_{1/2}$	−13.2	−13.0	−13
	$0p_{3/2}$	−2.5	−3.1	−1
	$0p_{1/2}$	−2.0	−2.8	−1

tem, while Table II compares the experimental and theoretical separation energies for ^{16}O and $^{16}_{\Lambda}$N. The resulting scalar and vector potentials are similar to what one obtains with a Hartree calculation using the $\sigma-\omega$ model, but lack the slight bump near the origin.

In the relativistic shell model it is mostly the combination $S(r)+V(r)$ that controls the location of the single-particle energy levels and, thus, behaves like a central term, whereas $S(r)-V(r)$ roughly determines the relative size of the spin-oribt splitting. This will be examined further in Sec. V where these combinations of $S(r)$ and $V(r)$ are shown to be the leading terms in a nonrelativistic reduction of the Dirac equation.

Since we evaluate our matrix elements in momentum space we proceed to Fourier transform the Dirac wave functions using standard techniques

$$\Psi^{\mu}_{\kappa}(\mathbf{p})=\frac{1}{(2\pi)^{3/2}}\int d^3r\, e^{-i\mathbf{p}\cdot\mathbf{r}}\Psi^{\mu}_{\kappa}(\mathbf{r}) =\frac{2}{\sqrt{2\pi}}(-i)^{l}\begin{bmatrix} f_{\kappa}(p)\chi^{\mu}_{\kappa}(\hat{\mathbf{p}},s) \\ -S_{\kappa}g_{\kappa}(p)\chi^{\mu}_{-\kappa}(\hat{\mathbf{p}},s)\end{bmatrix}, \quad (6)$$

where we have used $(-i)^{\bar{l}+1}=(-i)^{l}S_{\kappa}$ with $S_{\kappa}=\kappa/|\kappa|$, $\bar{l}(\kappa)=l(-\kappa)$ and we have dropped the radial quantum number n. The "radial" components in momentum space are given by

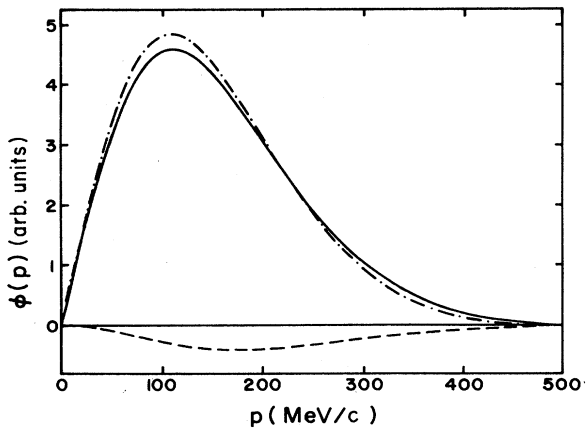

FIG. 1. "Radial" momentum space wave function of a $p_{3/2}$ proton showing the upper (solid curve) and lower (dashed curve) of the Dirac shell model spinor, and the equivalent Schrödinger wave function (dash-dotted curve).

$$f_{\kappa}(p)=\int_0^{\infty}r^2\,dr\, j_l(pr)f_{\kappa}(r)\,,$$
$$g_{\kappa}(p)=\int_0^{\infty}r^2\,dr\, j_{\bar{l}}(pr)g_{\kappa}(r)\,, \quad (7)$$

where, for simplicity, we denote the wave functions with f and g in coordinate as well as in momentum space. Figure 1 shows the $p_{3/2}$ proton wave functions in momentum space for ^{16}O. Note that for large momenta, the "small" and "large" relativistic components become comparable.

III. THE KAON OPTICAL POTENTIAL

In sharp contrast to the situation for pions, the average interactions of K^+ and K^- with nucleons, and hence also with nuclei, are very different in character,[5] particularly in the low- and intermediate-energy region ($p_{\rm lab}<1$ GeV/c). This difference is due to strangeness, a conserved quantum number for strong interactions which is $+1$ for K^+ and -1 for K^-.

The K^+N interaction is rather weak on the hadronic scale, corresponding to a mean free path in nuclear matter of roughly 5–7 fm, which is a typical nuclear size. This implies that low-energy K^+'s are capable of penetrating the nuclear interior, unlike the K^- and medium energy pions. Because of strangeness conservation, Y^*'s are not available as resonant or bound states of the K^+N system, nor are there any inelastic channels with the obvious exception of (K^+,K^0) charge exchange on neutrons. Consequently, the low-energy K^+N interaction can be understood by a rather simple background scattering, resulting in a smooth energy dependence of the cross sections. The large medium effects due to annihilation ($\pi NN\rightarrow NN$) and Δ resonance propagation, which enliven the π-nucleus system, are totally absent from the K^+-nucleus interaction.

In order to reduce the K^+-nucleus many-body problem to an equivalent potential scattering problem, an optical potential is constructed which has a less complicated structure than the pion nucleus optical potential.[21] For the interpretation of K^+ nuclear data, reliable analyses of the K^+N amplitudes are essential; they have been performed extensively, involving phase-shift analyses,[22] meson exchange models, and dispersion relations,[5] drawing from a large amount of experimental data.

Elastic scattering phase shifts, total cross sections, and distorted wave functions for reaction calculations are obtained by solving the Klein-Gordon equation

$$[-\nabla^2+\mu^2-(E-V_c)^2]\Psi(\mathbf{r})=-2EV(r)\Psi(\mathbf{r})\,, \quad (8)$$

where μ is the K^+ reduced mass, E is the total energy, and V_c is the Coulomb potential. Since phase-shift analyses indicate that s- and p-waves are most important in the energy regime $p_{\rm lab}<1$ GeV/c, $V(r)$ can be approximated by a potential of the Kisslinger type,

$$-2EV(r)=b_0\rho(r)-b_1\nabla\rho(r)\nabla \quad (9)$$

to first order in the nuclear densities.

The parameters are related to the average amplitude by

$$b_0=\frac{4\pi}{p_{\rm lab}}(kf_{\rm av}^{l=0})_{\rm c.m.}\ ,$$
$$b_1=\frac{4\pi}{p_{\rm lab}k^2}(kf_{\rm av}^{l=1})_{\rm c.m.}\ , \tag{10}$$

where $p_{\rm lab}$ and k are the laboratory and c.m. K^+ momenta, respectively, and

$$f_{\rm av}=\tfrac{1}{2}(f_{K^+p}+f_{K^+n})\ , \tag{11}$$

To include possible loss of kaon flux due to inelastic distortion such as multiple pion production, kaon plus delta excitation, etc., these parameters acquire imaginary parts; therefore, $\mathrm{Im}b_0$ and $\mathrm{Im}b_1$ represent the annihilation of s- and p-wave kaons in the nuclear medium. We note that we have neglected an additional charge exchange contribution $b_{\rm ce}[\rho_n(r)-\rho_p(r)]$ to Eq. (9),[5] where $b_{\rm ce}$ is given by

$$b_{\rm ce}=-\frac{2\pi}{p_{\rm lab}}k(f^{l=0}_{K^+n\to K^0p})_{\rm c.m.} \tag{12}$$

and probes isospin differences in the target nucleus. The parameters b_0 and b_1 are displayed in Figs. 2(a) and 2(b) as a function of the K^+ laboratory momentum $p_{\rm lab}$. We employ the phase shifts of Martin for the K^+N system,[22] since they have been more successful in reproducing K^+-nucleus elastic scattering data than other parametrizations. The strength b_0 is seen to be weakly energy dependent, while there is more variation for b_1, the parameter of the p-wave potential.

Since we perform our calculations in momentum space we need the Fourier transformation of the distorted kaon wave function. We do not repeat this computation here but refer to Ref. 15 which has formally derived the transformation of the distorted meson wave function into momentum space.

IV. MATRIX ELEMENTS IN THE RELATIVISTIC IMPULSE APPROXIMATION

Following the conventions of Bjorken and Drell,[23] the differential cross section for the reaction $\gamma+A\to K^++{}_\Lambda\mathrm{B}$ in the center of momentum (cm) frame can be written as

$$\frac{d\sigma}{d\Omega_K^{\rm c.m.}}=\frac{1}{16\pi^2}\frac{q^{\rm cm}}{k^{\rm cm}}\frac{m_im_f}{W^2}\frac{F_{\rm cm}}{2(2J_i+1)}\sum_{M_i,M_f,\lambda}|\langle J_fM_f,T_fN_f;K^+|T|J_iM_i,T_iN_i;\gamma\rangle|^2\ , \tag{13}$$

where we average over the initial spin projection M_i as well as the photon polarization λ and sum over the final spin projection M_f. The four-momenta of the photon and kaon are denoted by $(E_\gamma,\mathbf{k})$ and $(E_K,\mathbf{q})$; the total spins and isospins are J_i,J_f and T_i,T_f, respectively, along with their projections M_i,M_f and N_i,N_f. The usual correction factor compensating for the lack of translational invariance of the shell model is given by $F_{\rm cm}=\exp[b^2(\mathbf{k}-\mathbf{q})^2/2A]$, b being the harmonic oscillator parameter for the nucleus under study and A the nuclear mass number. The masses of the initial- and final-state nuclei are m_i and m_f, and W is the total energy in the cm system. In Fig. 3 the kinematic situation is presented in the laboratory frame, where the momentum transfer to the final-state nucleus is defined to be $\mathbf{Q}=\mathbf{k}-\mathbf{q}$.

The nuclear kaon production amplitude is taken to be a one-body operator in the baryon space, partly because it is the conventional starting point for calculations invoking the impulse approximation and because one hopes that two-step processes and meson exchange currents are small and can be incorporated in the future.

The basic matrix element is then given by

$$\langle J_fM_f,T_fN_f;K^+|T|J_iM_i,T_iN_i;\gamma\rangle=\sum_{\alpha,\alpha'}\langle J_fM_f,T_fN_f|C^\dagger_{\alpha'}C_\alpha|J_iM_i,T_iN_i\rangle\times\langle\alpha';K^+|t|\alpha;\gamma\rangle\ , \tag{14}$$

where $C^\dagger_{\alpha'}$ and C_α can be written as

$$C_\alpha=\theta(\epsilon_a-\epsilon_F)a_\alpha+\theta(\epsilon_F-\epsilon_a)S_\alpha b^\dagger_{-\alpha}\ , \tag{15}$$

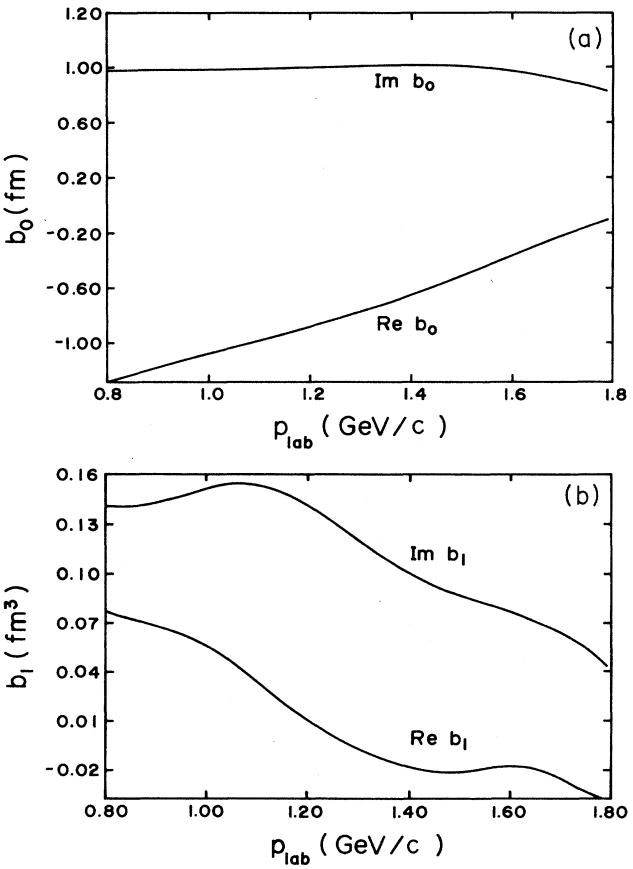

FIG. 2. The complex optical potential parameters $b_0(a)$ and $b_1(b)$ as a function of the kaon laboratory momentum.

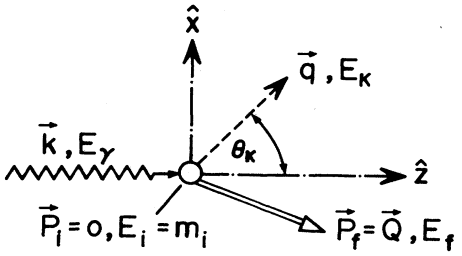

FIG. 3. Kinematics of $A(\gamma,K^+)_\Lambda B$ in the laboratory frame.

where a_α is the particle annihilation operator for energies ϵ_a above the Fermi energy ϵ_F and $b_{-\alpha}$ is the hole creation operator for energies below ϵ_F (excluding the Dirac sea). Here α denotes a set of quantum numbers for a single particle $\alpha=\{am;tm_t\}$ with $a=\{n\kappa\}$. $S_\alpha=(-1)^{j-m}(-1)^{t-m_t}$ is the phase necessary to maintain the transformation properties of the irreducible tensors.

In Eq. (14) the many-body nuclear structure aspects are already separated from the photoproduction mechanism but in principle the sum extends over a complete set of single-particle states α and α'. The nuclear structure information involved in one-body processes is usually contained in the double-reduced density matrix elements (RDME), defined by[24]

$$\Psi_{J;T}(a',a)=\hat{J}^{-1}\hat{T}^{-1}\langle J_f,T_f\|[C^\dagger_{\alpha'}\otimes\tilde{C}_\alpha]\|J_i,T_i\rangle\ , \tag{16}$$

where $\hat{x}=\sqrt{2x+1}$, $\tilde{C}_\alpha=S_\alpha C_{-\alpha}$, and J and T are the total spin and isospin transferred to the nucleus in the transition. Using the definition of Eq. (16), we evaluate the nuclear structure matrix element to obtain

$$\begin{aligned}\langle J_fM_f;T_fN_f|C^\dagger_{\alpha'}C_\alpha|J_iM_i;T_iN_i\rangle &= \sum_{\substack{J,M\\T,N}}(-1)^{j-m+(1/2)-m_t+J_i-M_i+T_i-N_i}\hat{J}^2\hat{T}^2 \\ &\times\begin{bmatrix}J_f & J_i & J\\ -M_p & M_i & M\end{bmatrix}\begin{bmatrix}T_f & T_i & T\\ -N_f & N_i & N\end{bmatrix}\begin{bmatrix}j' & j & J\\ -m' & m & M\end{bmatrix}\begin{bmatrix}t_y & \frac{1}{2} & T\\ -m_y & m_t & N\end{bmatrix}\Psi_{J;T}(a',a)\ ,\end{aligned} \tag{17}$$

where $t_y=0$ for the Λ.

Nonrelativistic RDME can either be obtained through shell model calculations, such as those of Cohen and Kurath for nuclei[25] and Ref. 26 for hypernuclei, or by using phenomenological methods constraining the nuclear matrix elements by experimental information.[27] Since nuclear structure calculations employing a Dirac single-particle basis are still in their beginning stages[28] we have adopted an extreme single-particle single-hole model, where a nucleon in a pure state α is transformed into a hyperon in a pure orbital α'. For a closed shell target nucleus in an extreme particle-hole basis, the RDME simply reduce to

$$\Psi_{J;T}(a',a)=\delta_{ab}\delta_{a'b'}\ . \tag{18}$$

All the dynamics of the photoproduction process is contained in the single-particle matrix element $\langle\alpha';K^+|t|\alpha;\gamma\rangle$ which in general involves a nonlocal and fully relativistic operator. In momentum space this matrix element has the form

$$\langle\alpha';K^+|t|\alpha;\gamma\rangle=\int d^3p\,d^3q'\bar{\psi}_{\alpha'}(\mathbf{p}')\phi_K^{*(-)}(\mathbf{q},\mathbf{q}')t_\gamma\psi_\alpha(\mathbf{p})\ , \tag{19}$$

where $\mathbf{p}'=\mathbf{p}+\mathbf{k}-\mathbf{q}$, $\bar{\psi}_{\alpha'}=\psi^\dagger_{\alpha'}\gamma_0$, and ψ_α is a single-particle solution of the Dirac equation given by Eq. (6). The wave function with the appropriate boundary conditions for the outgoing kaon of three-momentum $\mathbf{q}$ distorted by its interaction with the residual hypernucleus through an optical potential is $\phi_K^{(-)}(\mathbf{q}',\mathbf{q})$ and obeys the relation[29]

$$\phi_K^{*(-)}(\mathbf{q}',\mathbf{q})=\phi_K^{(+)}(\mathbf{q}',\mathbf{q})\ .$$

The representation of the matrix element in Eq. (19) is valid for any photoproduction amplitude based on diagrammatic techniques. We use a frame-independent operator that can be written as

$$t=\sum_{i=1}^{4}A_i(s,t)M_i\ , \tag{20}$$

where the gauge and Lorentz invariant matrices are given in terms of Dirac matrices and momentum four-vectors by

$$\begin{aligned}M_1&=-\gamma_5\not{\epsilon}\not{p}_\gamma\ ,\\ M_2&=2\gamma_5(\epsilon\cdot p_p p_\gamma\cdot p_\Lambda-\epsilon\cdot p_\Lambda p_\gamma\cdot p_p)\ ,\\ M_3&=\gamma_5(\not{\epsilon}p_\gamma\cdot p_p-\not{p}_\gamma\epsilon\cdot p_p)\ ,\\ M_4&=\gamma_5(\not{\epsilon}p_\gamma\cdot p_\Lambda-\not{p}_\gamma\epsilon\cdot p_\Lambda)\ ,\end{aligned} \tag{21}$$

with $\epsilon=(0,\boldsymbol{\epsilon})$ denoting the photon's polarization four-vector. The spin- and polarization-independent amplitudes A_i which are functions of the Mandelstam variables and the coupling constants are given in Ref. 14 apart from the terms arising from the $K1(1280)$ resonance in the t channel given by

$$A_1^{K1}=0\ ,$$

$$A_2^{K1}=\frac{1}{t-M_{K1}^2+iM_{K1}\Gamma_{K1}}\frac{-G_T^{K1}}{M_\Lambda+M_p}\ ,$$

$$A_3^{K1}=\frac{1}{t-M_{K1}^2+iM_{K1}\Gamma_{K1}}\left[G_V^{K1}+G_T^{K1}\frac{M_\Lambda-M_p}{M_\Lambda+M_p}\right]\ ,$$

$$A_4^{K1}=\frac{1}{t-M_{K1}^2+iM_{K1}\Gamma_{K1}}\left[-G_V^{K1}-G_T^{K1}\frac{M_\Lambda-M_p}{M_\Lambda+M_p}\right]\ .$$

It is important not to confuse these four-momenta, which are determined by conserving energy and momentum for the elementary process $\gamma+p\rightarrow K^++\Lambda$ in the nucleon's laboratory frame, with the momenta appearing in the hypernuclear formation cross section, which are evaluated in the many-body laboratory frame. Combining the transition amplitude t with γ_0 from the adjoint wave function yields the following matrix form of the operator:

$$\gamma_0 t=\begin{bmatrix}t_1 & t_2\\ t_3 & t_4\end{bmatrix}$$

$$=\begin{bmatrix}\boldsymbol{\sigma}\cdot\boldsymbol{\epsilon}(G_3-G_1)+G_4\boldsymbol{\sigma}\cdot\mathbf{k} & \frac{G_1}{k}\boldsymbol{\sigma}\cdot\boldsymbol{\epsilon}\,\boldsymbol{\sigma}\cdot\mathbf{k}+G_2-kG_4\\ \frac{-G_1}{k}\boldsymbol{\sigma}\cdot\boldsymbol{\epsilon}\,\boldsymbol{\sigma}\cdot\mathbf{k}-G_2-G_4k & \boldsymbol{\sigma}\cdot\boldsymbol{\epsilon}(G_1+G_3)+G_4\boldsymbol{\sigma}\cdot\mathbf{k}\end{bmatrix} \tag{22}$$

with

$$G_1=kA_1,\quad G_2=2A_2(\boldsymbol{\epsilon}\cdot\mathbf{p}'k\cdot p-\boldsymbol{\epsilon}\cdot\mathbf{p}k\cdot p'),\quad G_3=A_3k\cdot p+A_4k\cdot p',\quad G_4=A_3\boldsymbol{\epsilon}\cdot\mathbf{p}+A_4\boldsymbol{\epsilon}\cdot\mathbf{p}'\ , \tag{23}$$

where in the laboratory frame we have made the usual gauge choice of $\epsilon_0=0,\boldsymbol{\epsilon}\cdot\mathbf{k}=0$.

We obtain for the matrix element

$$\langle\alpha',K^+|t|\alpha,\gamma\rangle=\frac{2}{\pi}i^{l-l'}\int d^3p\,d^3q'\phi_K^{(-)*}(\mathbf{q},\mathbf{q}')(\rho_1\chi_\kappa^{\mu'\dagger}t_1\chi_\kappa^\mu-\rho_2S_\kappa\chi_{\kappa'}^{\mu'\dagger}t_2\chi_{-\kappa}^\mu-\rho_3S_{\kappa'}\chi_{-\kappa'}^{\mu'\dagger}t_3\chi_\kappa^\mu+\rho_4S_\kappa S_{\kappa'}\chi_{-\kappa'}^{\mu'\dagger}t_4\chi_{-\kappa}^\mu) \tag{24}$$

with the momentum overlap distributions defined as

$$\rho_1(p',p)=f_{\kappa'}(p')f_\kappa(p),\quad \rho_2=f_{\kappa'}g_\kappa\ ,$$
$$\rho_3=g_{\kappa'}f_\kappa,\quad \rho_4=g_{\kappa'}g_\kappa\ . \tag{25}$$

Each of the four operators t_n can be decomposed into spin-0 and spin-1 transition amplitudes

$$t_n=L_n+i\boldsymbol{\sigma}\cdot\mathbf{K}_n=\sum_{s,m_s}i^s(-1)^{m_s}\sigma^s_{-m_s}(K_n)^s_{m_s} \tag{26}$$

with

$$\sigma^0=1,\quad (K_n^0)=L_n\ ,$$

where the $S=1$ part contains the important Kroll-Rudermann term $\boldsymbol{\sigma}\cdot\boldsymbol{\epsilon}$. To simplify the angular momentum algebra, we also employ the relation

$$\frac{\boldsymbol{\sigma}\cdot\mathbf{p}}{|\mathbf{p}|}\chi_\kappa^\mu(\hat{\mathbf{p}})=-\chi_{-\kappa}^\mu(\hat{\mathbf{p}})\ . \tag{27}$$

Finally, by evaluating the single-particle matrix element in the LS coupling scheme where we couple the orbital angular momenta to L, the spins to S, and L and S to the total transition spin J, we obtain

$$\langle\alpha';K^+|t|\alpha;\gamma\rangle=\frac{4}{\pi}\sum_{L,S,J,M}\sum_{n=1}^{4}i^{S+l'-l+1}(-1)^{S+l'+j-\mu}\hat{j}\hat{j}'\hat{L}\hat{S}\hat{J}\begin{bmatrix}j' & j & J\\ -\mu' & \mu & M\end{bmatrix}\begin{Bmatrix}l' & \frac{1}{2} & j'\\ l & \frac{1}{2} & j\\ L & S & J\end{Bmatrix}I^{LSJ}_{-Mn}\ , \tag{28}$$

where the integrals are given by

$$I_{Mn}^{LSJ}=\int d^3p\, d^3q'\phi_K^{(-)*}(\mathbf{q},\mathbf{q}')\rho_n(p,p') \times[[Y_{l'}(\hat{\mathbf{p}}')\times Y_l(\hat{\mathbf{p}})]^L\times K_n^S]_M^J \ . \tag{29}$$

The tensor operators as well as the momentum distributions determine the magnitude and importance of the various matrix elements for the specific nuclear transition. While Refs. 30 and 31 provide compact analytic expressions for these operators for $J=0$, 1, 2, and 3, in general we use the definition of the tensor product to obtain

$$[[Y_{l'}(\hat{\mathbf{p}}')\times Y_l(\hat{\mathbf{p}})]^L\times K_n^S]_M^J = \sum_{\substack{m,m'\\ M_L,M_S}} (l'lm'm|LM_L)(LSM_LM_S|JM) \times Y_{l'}^{m'}(\hat{\mathbf{p}}')Y_l^m(\hat{\mathbf{p}})K_{nM_S}^S \ . \tag{30}$$

The $S=0$ and 1 transition amplitudes L_n and $\mathbf{K}_n$ can be written as

$$\begin{aligned}
&L_1=0 \ ,\\
&\mathbf{K}_1=-[(G_3-G_1)\boldsymbol{\epsilon}+G_4\mathbf{k}] \ ,\\
&L_2=\frac{S_\kappa}{p}\mathbf{p}\cdot(\boldsymbol{\epsilon}\times\mathbf{k})\frac{G_1}{k} \ ,\\
&\mathbf{K}_2=-\frac{S_\kappa}{2}\{\mathbf{p}(G_2-kG_4)+\frac{G_1}{k}[\boldsymbol{\epsilon}(\mathbf{p}\cdot\mathbf{k})-\mathbf{k}(\mathbf{p}\cdot\boldsymbol{\epsilon})]\} \ ,\\
&L_3=-\frac{S_{\kappa'}}{p'}\mathbf{p}'\cdot(\boldsymbol{\epsilon}\times\mathbf{k})\frac{G_1}{k} \ ,\\
&\mathbf{K}_3=\frac{S_{\kappa'}}{p'}\{\mathbf{p}'(G_2+kG_4)+\frac{G_1}{k}[\mathbf{k}(\mathbf{p}\cdot\boldsymbol{\epsilon})-\boldsymbol{\epsilon}(\mathbf{p}'\cdot\mathbf{k})]\} \ ,\\
&L_4=\frac{S_\kappa S_{\kappa'}}{pp'}[(G_1+G_3)\mathbf{p}'\cdot(\boldsymbol{\epsilon}\times\mathbf{p})+G_{4p'}\cdot(\mathbf{k}\times\mathbf{p})] \ ,\\
&K_4=\frac{S_\kappa S_{\kappa'}}{pp'}\{(G_1+G_3)[\boldsymbol{\epsilon}(\mathbf{p}'\cdot\mathbf{p})-\mathbf{p}(\mathbf{p}'\cdot\boldsymbol{\epsilon})-\mathbf{p}'(\boldsymbol{\epsilon}\cdot\mathbf{p})] \\
&\qquad +G_4[\mathbf{k}(\mathbf{p}'\cdot\mathbf{p})-\mathbf{p}(\mathbf{p}'\cdot\mathbf{k})-\mathbf{p}'(\mathbf{p}\cdot\mathbf{k})]\} \ ,
\end{aligned} \tag{31}$$

where the G_i are given in Eq. (23) in terms of the elementary amplitudes A_i. Combining the nuclear structure matrix elements [Eq. (17)] with the single-particle matrix elements [Eq. (28)], we can carry out the spin projection summations to obtain

$$\sum_{M_i,M_f,\lambda}|\langle J_fM_f;T_fN_f;K^+|T|J_iM_i;T_iN_i;\gamma\rangle|^2 = \sum_{J,M,\lambda}|F_M^J|^2 \ ,$$

with

$$F_M^J=\sum_{L,S,n}(-i)^S\hat{j}'\hat{j}\hat{L}\hat{S}\begin{Bmatrix} l' & \frac{1}{2} & j' \\ l & \frac{1}{2} & j \\ L & S & J \end{Bmatrix} I_{Mn}^{LSJ} \ , \tag{32}$$

where the sum over the complete set of states a' and a has been eliminated by the delta function in Eq. (18).

V. NONRELATIVISTIC REDUCTIONS

In an attempt to compare the relativistic approach with conventional calculations which employ the Schrödinger equation to describe single-particle motion in the nucleus, we require the matrix elements and, in particular, the operator that is given in terms of Dirac matrices to undergo a nonrelativistic reduction to Pauli spin space. However, expansion in powers of p/M and omission of higher-order terms may not always give us a unique prescription,[32,33] since operators derived from fully relativistic diagrammatic principles consist of propagators, vertex functions, and Dirac spinors, and it is not clear at what stage of the derivation the approximation should be performed. The effects from different nonrelativistic reductions are small as long as $p \ll M$, which is not the case for kaon photoproduction. As discussed extensively in the literature,[17–19] the first step in a nonrelativistic reduction is the replacement of E^*+M^* [where $E^*=E-V(r)$ and $M^*=M+S(r)$] by their free values $E+M$, which leads to

$$\psi=\begin{bmatrix} \phi \\ \dfrac{\boldsymbol{\sigma}\cdot\mathbf{p}}{E^*+M^*}\phi \end{bmatrix}\rightarrow\begin{bmatrix} \phi \\ \dfrac{\boldsymbol{\sigma}\cdot\mathbf{p}}{E+M}\phi \end{bmatrix}=u(\mathbf{p})\phi \ . \tag{33}$$

The amplitude can now be evaluated between the free spinors $\bar{u}(\mathbf{p}')$ and $u(\mathbf{p})$, emerging as an operator in Pauli space. In the nuclear interior

$$g_\kappa^{\text{bound}}\sim\frac{E+M}{E+M-V_0+S_0}g_\kappa^{\text{free}} \tag{34}$$

and most relativistic models find $V_N\sim 300$ MeV and $S_N\sim -400$ MeV for the nucleon,[20] and $V_\Lambda\sim 110$ MeV and $S_\Lambda\sim -150$ MeV for the lambda.[34] Therefore, the small component is enhanced by about 1.7 for the nucleon but only 1.1 for the lambda as a direct consequence of these large nuclear potentials.

The upper component of the Dirac spinor is usually identified with a nonrelativistic wave function. However, a reduction of the Dirac equation to an equivalent Schrödinger equation[35] introduces not only the standard state-dependent central and spin-orbit potentials but also an energy-dependent term containing derivatives. This shows that a Dirac equation with local, state-independent potentials implicitly contains nonlocalities and energy dependencies not present in the conventional nonrelativistic wave equation.

To obtain a nonrelativistic amplitude that is to be used with Schrödinger wave functions, the relativistic operator of Eq. (20) needs to be evaluated between free Dirac spinors in order to reduce it to Pauli spin space. It has been shown previously[14,28] that the static $\boldsymbol{\sigma}\cdot\boldsymbol{\epsilon}$ operator should not be used in a nuclear calculation, while dropping terms of order p^2/M^2 coming from the spinors provides a good approximation to the full operator. The integral I_M^{LSJ} of Eq. (29) in an entirely nonrelativistic calculation are then obtained by setting $n=1$ where

$$\rho(p',p)=\psi_{n'l'j'}(p')\psi_{nlj}(p)$$

is the density of some nonrelativistic wave functions and the nonrelativistic operator K_{nr}^S can be written in terms

of the G_i defined in Eq. (26)

$$L_{\rm nr}=\frac{G_1}{2k}\left[\frac{1}{M_p}\mathbf{p}\cdot(\boldsymbol{\epsilon}\times\mathbf{k})-\frac{1}{M_\Lambda}\mathbf{p}'\cdot(\boldsymbol{\epsilon}\times\mathbf{k})\right],$$

$$\mathbf{K}_{\rm nr}=-\boldsymbol{\epsilon}\left[G_3-G_1+\frac{G_1}{2k}\left[\frac{\mathbf{k}\cdot\mathbf{p}}{M_p}+\frac{\mathbf{k}\cdot\mathbf{p}'}{M_\Lambda}\right]\right]$$
$$+\mathbf{k}\left[\frac{G_1}{2k}\left[\frac{\boldsymbol{\epsilon}\cdot\mathbf{p}}{M_p}+\frac{\boldsymbol{\epsilon}\cdot\mathbf{p}'}{M_\Lambda}\right]-G_4\right]$$
$$-\mathbf{p}\left[\frac{G_2-kG_4}{2M_p}\right]+\mathbf{p}'\left[\frac{G_2+kG_4}{2M_p}\right], \tag{35}$$

where we have used $E_\Lambda\approx M_\Lambda$ and $E_p\approx M_p$ and discarded contributions coming from products of the small components, since they are of order p^2/M^2. Note, that previous nonrelativistic calculations have only included the $\boldsymbol{\sigma}\cdot\boldsymbol{\epsilon}$ part of the operator $\mathbf{K}_{\rm nr}$, and $L_{\rm nr}$ which is responsible for non-spin-flip transitions was neglected entirely.

VI. PLANE WAVE AND LOCAL APPROXIMATIONS

It is useful to discuss some approximations to the single-particle matrix element [Eq. (28) and (29)] that are commonly made. Using the free kaon solution, which is a delta function in momentum space

$$\phi_K^{(+)}(\mathbf{q},\mathbf{q}')=\delta(\mathbf{q}'-\mathbf{q}), \tag{36}$$

we arrive at the nonlocal relativistic plane wave impulse approximation (RPWIA) result

$$I_{Mn}^{LSJ}=\int d^3p\,\rho_n(p',p)[[Y_{l'}(\hat{\mathbf{p}}')\times Y_l(\hat{\mathbf{p}})]^L\times K_n^S]_M^J \tag{37}$$

with the densities ρ_n given by Eq. (25) and the operators K_n^S given by Eq. (31).

There are several possibilities in going from a full nonlocal to a local computation. In coordinate space nonlocalities can be partially included by replacing $\mathbf{p}\rightarrow -i\nabla_p$, acting on the bound-state wave function, and $\mathbf{q}\rightarrow -i\nabla_q$, acting on the kaon wave function; however, this method ignores the momentum dependence of the propagators. We reduce K_n^S to local operators by fixing the initial nucleon momentum $\mathbf{p}$ to a certain constant value, which may be either zero (frozen nucleon approximation) or some average Fermi momentum. In the relativistic case, however, caution is required since the operators K_n^S in Eq. (31) contain parts of the single-particle wave function via the relation (27). Therefore, the local operators K_n^S will have to be redefined from the original amplitudes t_n in Eq. (22).

Using the partial wave expansion for the kaon solution as well as for the photon, we arrive at the local relativistic distorted wave impulse approximation (RDWIA) result

$$F_M^J=4\pi\hat{j}'\hat{j}\sum_{\substack{L,S\\ l_\gamma,l_K}}\sum_{n=1}^{4} i^{S+l_\gamma+l_K}(-1)^{l_K+L+S}\hat{L}\hat{S}\hat{l}_\gamma\hat{l}_K\hat{l}'_i\hat{l}_i\begin{bmatrix} l_\gamma & l_K & L\\ 0 & 0 & 0\end{bmatrix}\begin{bmatrix} l'_n & l_n & L\\ 0 & 0 & 0\end{bmatrix}\begin{Bmatrix} l'_n & \frac{1}{2} & j'\\ l_n & \frac{1}{2} & j\\ L & S & J\end{Bmatrix}$$
$$\times[[Y_{l_\gamma}(\hat{\mathbf{k}})\times Y_{l_K}(\hat{\mathbf{q}})]^L\times\tilde{K}_n^S]_M^J\int r^2dr\,\rho_n(r)U_{l_K,q}(r)j_{l_\gamma}(kr), \tag{38}$$

where

$$l_1,l_3=l,\quad l'_1,l'_2=l',\quad l_2,l_4=\bar{l},\quad l'_3,l'_4=\bar{l}'.$$

$U_{l_K,q}(r)$ is the kaon radial wave function and the $\rho_n(r)$ are now local densities in coordinate space,

$$\rho_1(r)=f_{\kappa'}(r)f_\kappa(r),\quad \rho_2=f_{\kappa'}g_\kappa,\quad \rho_3=g_{\kappa'}f_\kappa,\quad \rho_4=g_{\kappa'}g_\kappa. \tag{39}$$

The operators $\tilde{K}_n^S$ are now local and can be written as

$$L_1=\tilde{L}_4=0,\quad \tilde{L}_2=G_2-kG_4,\quad \tilde{L}_3=G_2+kG_4,$$
$$\tilde{\mathbf{K}}_1=\mathbf{K}_1,\quad \tilde{\mathbf{K}}_3=\tilde{\mathbf{K}}_2=\frac{G_1}{k}(\boldsymbol{\epsilon}\times\mathbf{k}),\quad \tilde{\mathbf{K}}_4=-[(G_1+G_3)\boldsymbol{\epsilon}+G_4\mathbf{k}]. \tag{40}$$

If kaon distortions are neglected, the plane waves from the photon and the kaon can be combined, simplifying the expression for the local RPWIA

$$F_M^J=\sqrt{4\pi}\hat{j}'\hat{j}\sum_{L,S}\sum_{n=1}^{4}(-1)^{S+L}\hat{L}\hat{S}\hat{l}'_n\hat{l}_n\begin{bmatrix} l'_n & l_n & L\\ 0 & 0 & 0\end{bmatrix}\begin{Bmatrix} l'_n & \frac{1}{2} & j'\\ l_n & \frac{1}{2} & j\\ L & S & J\end{Bmatrix}[Y_L(\hat{\mathbf{Q}})\times\tilde{K}_n^S]_M^J\int r^2dr\,\rho_n(r)j_L(Qr), \tag{41}$$

where $\mathbf{Q}=\mathbf{k}-\mathbf{q}$ is the momentum transfer to the nucleus. The nonrelativistic expressions can be obtained from the relativistic formulas (37), (38), and (41) by taking only the term for $n=1$, using nonrelativistic wave functions for the density ρ_1 and employing the nonrelativistic operator $K^S_{\rm nr}$ of Eq. (35) throughout.

VII. RESULTS AND DISCUSSION

Rather than examining a large number of specific kaon production reactions from a number of nuclei, we investigate the effects arising from different elementary operator descriptions, kaon distortions, nonlocal contributions from the operator and from Fermi motion, and the use of relativistic baryon wave functions for the bound single-particle orbits for the p-shell nucleus ^{16}O. The initial state is doubly closed and would only be modified by $2p$-$2h$ admixtures from the sd shell and we can restrict the configuration space in the final state to a closed $1s$-shell core and an open $1p$ shell for the nucleons, while the lambda goes into an s or p orbit. We have neglected the ΛN residual interaction including coupling to the continuum as considered by Rosenthal *et al.*[8] This clearly may lead to some energy shifts in lambda states, although strongly bound lambda states in p-shell nuclei and high-spin transitions are relatively unaffected.[8] It is very unlikely that the resolution of the early experiments will be able to separate energy levels split by this interaction. In any case, our calculation can handle more complicated factor $\Psi_{J,T}(a',a)$ given in Eq. (16) should this prove to be necessary.

For the purposes of our current investigations we describe ^{15}N as a pure $p_{1/2}$ proton hole coupled to an s- or p-shell lambda to form the various states in $^{16}_{\Lambda}$N. The ground-state configurations arise from a $p_{1/2}$ proton hole and a $s_{1/2}$ lambda coupling to a 0^- and a 1^- state. This degeneracy would most likely be removed in a realistic calculation that includes the ΛN residual interaction although the splitting is unlikely to be very large, so as noted above first generation experiments most likely cannot resolve the two states. At higher energies around 11 and 17 MeV one encounters substitutional transitions that take place only within the $1p$ shell. The splitting between the cluster of states belonging to the $(p^{-1}_{1/2},p_{3/2})$ and $(p^{-1}_{1/2},p_{1/2})$ configurations will provide important information about the lambda spin-orbit interaction if it is larger than the splittings induced by the ΛN residual interactions.

The remaining states, which involve an s-shell proton hole are at much higher energies ($E_x\approx 20$–30 MeV) and may be difficult to resolve since they are above the quasi-free production threshold.

The reaction (γ,K^+) from nuclei unlike the (π^+,K^+) reaction can strongly excite $S=1$ transitions. In terms of the spin-flip and non-spin-flip operators defined in Eq. (26), the differential cross section for the elementary process $\gamma+p\rightarrow K^++\Lambda^0$ can be written as

$$\frac{d\sigma}{d\Omega_K^{\rm cm}}=\frac{1}{32\pi^2}\frac{q^{\rm cm}M_pM_\Lambda}{k^{\rm cm}W^2}\sum_\lambda(|L|^2+|\mathbf{K}|^2)\ , \tag{42}$$

which shows the well-known fact that the $S=J=0$ and $S=J=1$ terms contribute equally to the cross section. This is not the case for kaon production from nuclei where selection rules can eliminate the $S=0$ or $S=1$ contributions in certain transitions. For example, in several of the high-spin and unnatural parity transitions leading to the states in $^{16}_{\Lambda}$N such as $(p^{-1}_{3/2},s_{1/2})2^-$ or the $(p^{-1}_{3/2},p_{3/2})3^+$ state only the spin-flip operator can contribute. Low-spin transitions proceed mainly through the $S=0$ part of the operator and, therefore, can test the non-spin-flip piece of the amplitude although most of these states have small cross sections. The only pure $S=0$ transition goes to the $(s^{-1}_{1/2},s_{1/2})0^+$ state which is at rather high excitation energy and is probably not observable.

The momentum transfer for kaon photoproduction from nuclei near threshold (which is 684 MeV for ^{16}O and less for heavier nuclei) is above 500 MeV/c and produces very small cross sections. For zero-degree kaons, the momentum transfer decreases monotonically with increasing photon energy while for kaons a few degrees away from zero degrees the momentum transfer reaches a minimum and then increases. For kaons within a forward cone of about 15°, a reasonable compromise is to consider $E^\gamma_{\rm lab}=1.5$–2.0 GeV with a Q value at 0° of 250–300 MeV/c. Figure 4 shows the angular distribution of kaons populating the $(p^{-1}_{1/2},s_{1/2})1^-$ state at $E^\gamma_{\rm lab}=0.84$, 1.0, 1.5, and 2.0 GeV calculated in the relativistic impulse approximation. For higher photon energies, the cross sections are larger at very small kaon angles, but fall off much faster at larger angles. At 840 MeV, an energy the Mainz Microton project will have available, the cross section ranges from 5–30 nb/sr for kaon angles up to 20°.

In Fig. 5 we show the energy dependence of the total cross section and differential cross section at 0° for the $1^-_{\rm g.s.}$ and 3^+ transitions. Contrary to the increasing forward cross section, the total cross section remains about

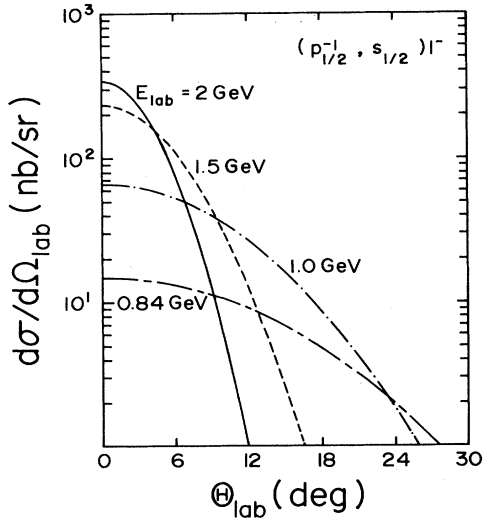

FIG. 4. Angular distributions for the $(p^{-1}_{1/2},s_{1/2})1^-$ ground state at different photon energies.

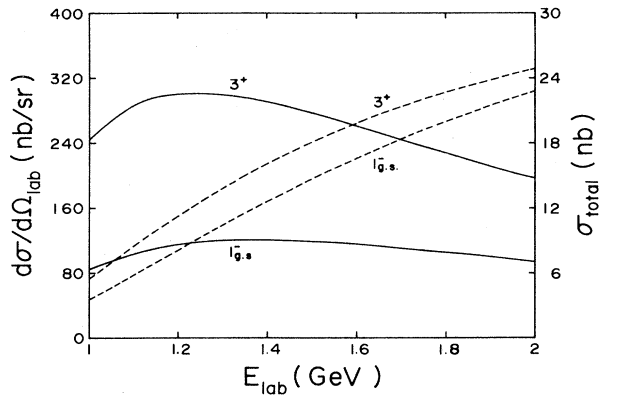

FIG. 5. Total (solid curve) and differential (dashed curve) cross sections at $\theta_K=0°$ for the $1^-_{g.s.}$ and the 3^+ transition as a function of the photon laboratory energy.

constant from 1.2–1.8 GeV and slowly decreases at higher energies. This suggests that for experiments employing a large solid angle detector energies considerably lower than the previously recommended 1.5–2.0 GeV are favorable.

Before addressing the significance of relativistic wave functions and kaon distortion, we examine the sensitivity of the kaon photoproduction from nuclei to different elementary amplitudes which all describe the free process $p(\gamma,K^+)\Lambda$ reasonably well.

In all the models considered below, pseudoscalar (PS) coupling was used for the $K\Lambda N$ vertex. In Ref. 36, we showed that using the Born terms only in pseudovector (PV) coupling agreement with data can only be obtained by refitting the coupling constants resulting in a change of their values by 20–30 % in contrast to pion photoproduction where both coupling models give identical predictions for the basic process.[31] If the operator for $p(\gamma,K^+)\Lambda$ is not readjusted, PV calculations overpredict the data by a factor of 2–3, which leads to large effects when the amplitude is used in nuclear calculations.[37] This surprising result may be due to the much larger kaon mass. However, if one uses effective operators that were obtained phenomenologically by a fit to the data, the difference between the PS and PV results are small. Even though PV coupling is known to, in general, yield more moderate relativistic effects in the nucleus, in this process both operators have the same structure in Dirac space as given in Eq. (21). They only differ by a constant term in the amplitude A_1 which is compensated by smaller coupling constants in the case of PV theory. More discussion on this problem can be found in Refs. 36 and 37.

We show results using the coupling constants of Thom[38] with the Born terms only (which include K^* and Σ exchange terms), the Adelseck, Bennhold, and Wright (ABW) II coupling constants[14] and resonances, which are a fit to photoproduction data with the Born terms plus two s-channel spin-$\frac{1}{2}$ resonances, the new Adelseck and Wright (AW) III results[13] which include the kaon resonance $K1(1280)$ in the t channel and an additional u-channel resonance term, and the AW IV results[13] which fit both photoproduction and electroproduction data. The electroproduction data from the proton determines the primary coupling constant $g_{K\Lambda N}$ rather well through a very consistent data set as compared to the photoproduction data set and confirms former determinations of the kaon radius.[13] The value of the primary constant $g_{K\Lambda N}$ determined by the electroproduction fit is in general agreement with values determined by hadronic processes, and the inclusion of the $K1(1280)$ t channel resonance in the photoproduction fit increases the value determined from photoproduction analyses to a similar value. These results resolve a long-standing concern that $g_{K\Lambda N}$ determined from electromagnetic interactions was considerably smaller than the value extracted from hadronic reactions or predicted by quark models. Using a different method, Tanabe *et al.*[39] can also recover the hadronic value for $g_{K\Lambda N}$ by including $K^+\Lambda$ final-state correlations in the free process through a conventional absorptive factor in each partial wave. This method can only be applied in the kaon-lambda cm frame and, thus, the calculational framework of evaluating momentum space matrix elements with operators in an arbitrary frame is lost. In Table III we give the four sets of coupling constants under investigation in this paper.

Figure 6 illustrates the sensitivity of hypernuclear formation to different elementary operators for the 3^+ and $0^-_{g.s.}$ transitions. The cross sections for the 3^+ transition at very forward angles are roughly similar, except that the magnitude varies by almost a factor of 2 and the shape from the AW IV amplitude is quite different. Fermi motion effects are small for 0° kaons and, therefore, the hypernuclear cross section is roughly proportional to the elementary cross section provided the $\sigma\cdot\epsilon$ term is dominant as in the 3^+ transition. At larger kaon angles the curves fall off differently indicating an increased sensitivity to the details of the operators. The predictions of the different amplitudes differ even more dramatically from each other in the case of the 0^- transition. Here the amplitude with the largest value for $g_{K\Lambda N}$ (AW III) predicts the highest counting rates, while ABW II with the smallest $K\Lambda N$-coupling constant yields the lowest cross section. On the other hand, the shapes and the po-

TABLE III. Coupling constants for the reaction $p(\gamma,K^+)\Lambda^0$.

Set	$\frac{g_\Lambda}{\sqrt{4\pi}}$	$\frac{G_\Sigma}{\sqrt{4\pi}}$	$\frac{G_V}{4\pi}$	$\frac{G_T}{4\pi}$	$\frac{G_V^{K1}}{4\pi}$	$\frac{G_T^{K1}}{4\pi}$	$\frac{G_{N_1}}{\sqrt{4\pi}}$	$\frac{G_{N_2}}{\sqrt{4\pi}}$	$\frac{G_Y}{\sqrt{4\pi}}$	Ref.
Thom	2.57	1.52	0.105	0.064	0	0	0	0	0	38
ABW II	1.03	−0.807	0.220	−0.048	0	0	1.47	0.111	0	14
AW III	4.30	3.60	0.124	−0.338	0.269	0.829	−0.907	0.103	3.35	13
AW IV	3.15	3.28	0.027	−0.188	0.132	0.063	−1.11	0.101	0.698	13

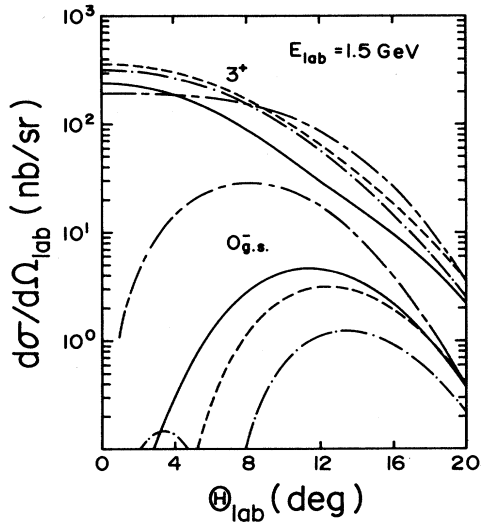

FIG. 6. Angular distributions for the $0^-_{g.s.}$ and 3^+ state with the coupling constants of Thom (— — —), ABW II (—·—·—·), AW III (— - — -), and AW IV (——) of Table IV.

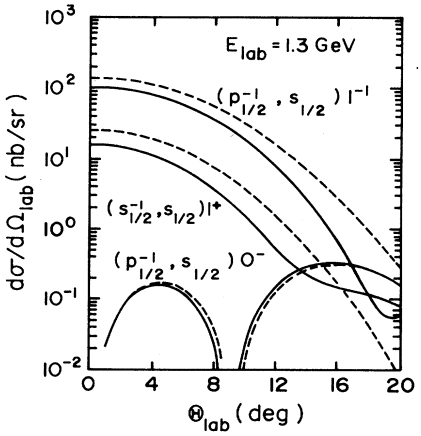

FIG. 7. Comparison of nonlocal DWIA (solid curves) with nonlocal PWIA (dashed curves) calculations for various transitions to $^{16}_{\Lambda}$N.

sitions of the minima are quite different for the four curves, and clearly cannot be simulated by just rescaling the dominant coupling. We found the behavior shown in Fig. 6 in a number of other transitions; namely differences of almost a factor of 2 between different operators for high-spin states with large cross sections and very large differences in magnitude and shape for the lower spin states. This situation clearly calls for new experimental efforts to measure the elementary production process more precisely in order to unambiguously determine the elementary amplitude. If not otherwise mentioned, we will use AW IV in this paper.

The inclusion of kaon distortion in a momentum space calculation requires the numerical evaluation of the six-dimensional integral given in Eq. (29). In investigating convergence, we varied the number of integration points over a wide range and found that precision of 2% was obtainable with about 200 000 integration points. This comparatively small number of integration points (pion photoproduction at energies from threshold up to the delta region from p-shell nuclei requires approximately 300 000 integration points for the same integrals[15]) was obtainable since the phase space for the rescattering K^+ (the variable $\mathbf{q}'$) can be restricted to a small cone about the asymptotic momentum $\mathbf{q}$ since kaon rescattering at backward angles gives only negligible contributions. This compensated for the fact that for photons around 1.5 GeV, the K^+ is highly energetic ($T^K \approx 700$ MeV) and requires about 25 partial waves to describe the outgoing kaon sufficiently accurately.

As expected from the discussion in Sec. III, the effects of kaon distortion are small for p-shell nuclei. In Fig. 7 we compare the full nonlocal distorted wave impulse approximation (DWIA) calculation with nonlocal plane wave impulse approximation (PWIA) and find differences of the order 20–30 % for a number of hypernuclear transitions. The high-spin states are uniformly scaled down, while for the lower spin states kaon distortion can slightly modify the shape of the curves. We show only nonrelativistic results in Fig. 7, since we find that kaon distortion affects the relativistic calculations in the same way. Note that we have not included the Coulomb distortion of the K^+ in our nonlocal DWIA calculations, but since our calculations are far away from threshold this neglect of Coulomb distortion is of minor importance for p-shell nuclei. The size of our distortion effects in p-shell nuclei is comparable to that quoted by Rosenthal *et al.*[8]

While the small effects of K^+ distortion in p-shell nuclei comes as no surprise, this situation will clearly change when one proceeds to heavier nuclei. The reaction ^{208}Pb$(\gamma,K^+)^{208}_{\Lambda}$Tl has been mentioned as a useful probe of possible modification of hadronic properties in nuclear matter. One might envision testing the modification of electromagnetic currents by measuring the magnetic moment of a deeply bound hyperon via ^{209}Bi$(\gamma,K^+)^{209}_{\Lambda}$Pb (Ref. 40) in order to compare it with that of the free lambda. Studying the nonmesonic decay channel $N\Lambda \rightarrow NN$ dominant for heavy nuclei may reveal information about the weak interaction in a situation close to nuclear matter. As shown in Fig. 8, however, K^+ distortion effects are large for the $A=208$ system, reducing cross sections by a factor of 3 or more in a local calculation. As pointed out in Ref. 8, configuration mixing should be much more important in a heavy system and may result in additional reductions. We do not see the need for an experiment on the $A=208$ system, but suggest that targets around $A=40$ should suffice to study the properties of a lambda bound in the $1s_{1/2}$ shell. Figure 8 shows that kaon distortion for the $A=40$ system only leads to a reduction of about a factor 2 in cross section. A possible alternative reaction to investigate modification of the lambda moment is ^{45}Sc$(\gamma,K^+)^{45}_{\Lambda}$Ca. Note that all of our calculations outside the p shell are local since we have not yet prepared our code for higher configurations but plan to do so in the future.

To assess the significance of relativistic effects, we compare calculations using Dirac wave functions and a full

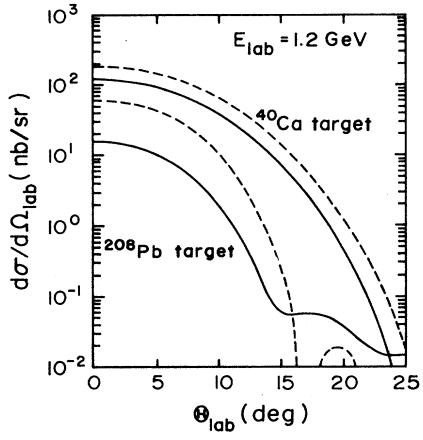

FIG. 8. Comparison of local DWIA (solid curves) with PWIA (dashed curves) calculations for the reactions ^{40}Ca$(\gamma,K^+)^{40}_{\Lambda}$K $(4^-_{g.s.})$ and ^{208}Pb$(\gamma,K^+)^{208}$Tl $(6^-_{g.s.})$.

relativistic production operator with computations performed in a nonrelativistic framework as outlined in Sec. V; that is, we use the free relation between the upper and lower components, identify the upper component with a conventional Schrödinger-type solution, and employ a p^2/m^2 reduction of the operator. Using the Dirac equation in nuclear reactions has proved most successful in predicting spin observables of proton-nucleus scattering, while the effects in photonuclear and electronuclear reactions have been less pronounced. We have not modified the propagators contained in the elementary operator inside the nucleus. These medium modifications of the basic amplitude go beyond the impulse approximation and are outside the scope of this work. Such modifications might bring about large effects as suggested in Ref. 28. However, a proper inclusion of medium modifications is a lengthy computation.

Figure 9 compares the relativistic and nonrelativistic computations for the 1^- and 0^- ground state. While for very forward angles the relativistic calculation is about 20% larger than the nonrelativistic one, the differences are more pronounced at larger angles. Dramatic differences can be observed for the 0^- state. Not only is the relativistic cross section larger by an order of magnitude, but the position of the minimum is shifted considerably. Even though the 1^- and 0^- states may not be resolvable energetically, the angular distributions based on a relativistic and nonrelativistic approach might be distinguishable at larger kaon angles since one would measure the incoherent sum of the 0^- and 1^- cross sections. In Fig. 10 we show the differences between relativistic and nonrelativistic calculations for a number of excited states with the configuration $(p^{-1}_{3/2},p_{3/2})$ allowing transitions with $J=0^+$, 1^+, 2^+, and 3^+ which are all degenerate in our model. Again, the 3^+ transition with the largest cross section is only affected at larger kaon angles while the low-spin states experience greater sensitivity. We found this behavior for a number of other transitions as well. These results can be understood by the fact that the high-spin states are dominated by the $\sigma\cdot\epsilon$ term which is part of the operator K_1 in Eq. (31) and is insensitive to the lower components of the Dirac spinors that are strongly modified in the relativistic formulation. Low-spin transitions proceed mainly through the $S=0$ or non-spin-flip part of the operator which is of order p/m and thus affected by a relativistic calculation. However, the differences between the relativistic and nonrelativistic cross sections are still subject to the elementary photoproduction amplitude. Using Thom's or ABW II coupling constants yields larger relativistic effects even for the high-spin transitions, as has been reported earlier.[12] Thus, the final conclusion on whether relativity is important can only be drawn after the elementary process is better understood.

In Fig. 11 we assess the validity of using a nonrelativistic operator for a calculation with Schrödinger wave

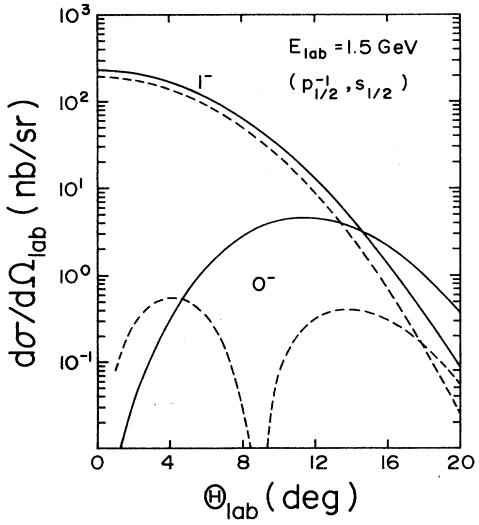

FIG. 9. Angular distributions for the 0^- and 1^- ground state comparing the relativistic (solid curve) and nonrelativistic (dashed curve) calculation.

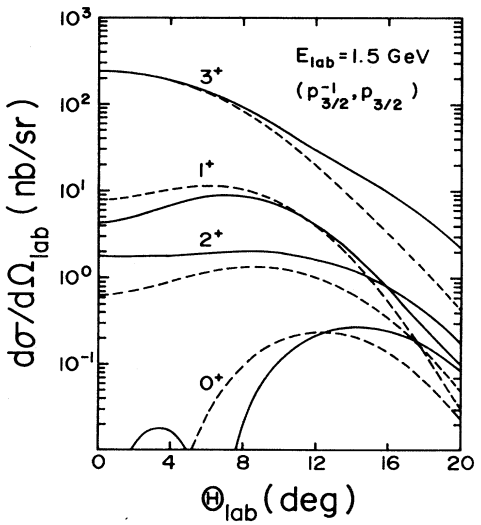

FIG. 10. Same as Fig. 7 for the 0^+, 1^+, 2^+, and 3^+ states with the $(p^{-1}_{3/2},p_{3/2})$ configuration.

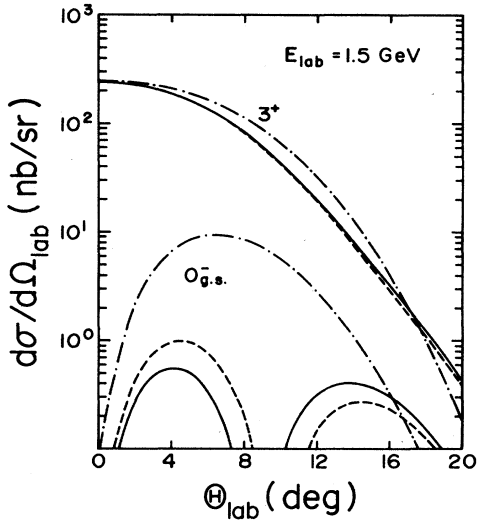

FIG. 11. Comparing different approximations to the elementary operator for the $0^-_{g.s.}$ and the 3^+ transition in a nonrelativistic calculation, using the full operator (— — —), a nonrelativistic operator (——), and the $\sigma\cdot\epsilon$ term only (—·—·—·).

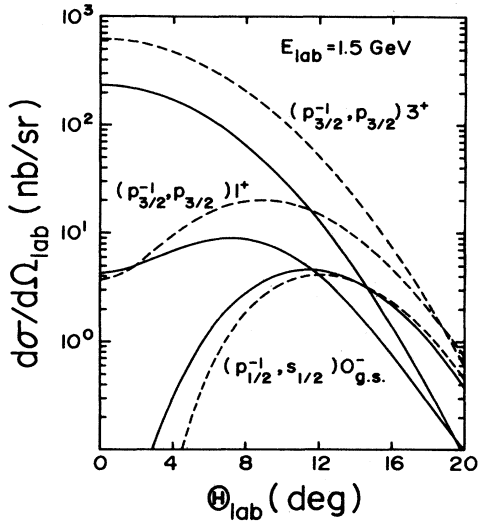

FIG. 12. Comparison of the nonlocal calculation (solid curve) with the local frozen proton approximation (dashed curve) computed in the relativistic framework.

functions. We compare the operator of Eq. (35) in which contributions from the products of the small spinor components have been dropped with the full operator and a calculation performed with the $\sigma\cdot\epsilon$ term only. For the 3^+ transition, there are no differences between the different computations for 0° kaons. Away from 0°, the $\sigma\cdot\epsilon$ term only shows deviations from the full operator while the nonrelativistic operator of Eq. (35) is in excellent agreement with the relativistic amplitude. Details of the operator are clearly important for the 0^- transition. While some effects show up already when using the nonrelativistic operator, retaining only the $\sigma\cdot\epsilon$ term overpredicts the cross section by an order of magntiude and cannot reproduce the minimum of the form factor.

We have calculated the cross section for various transitions with Woods-Saxon wave functions and harmonic oscillator wave functions for ^{16}O. The deeply bound lambda state is equally well described by the two wave functions, while the p-shell lambda which enters the 3^+ transition and is bound by about $\frac{1}{2}$ MeV is not adequately described by the harmonic oscillator wave function. We recommend using Woods-Saxon–type wave functions for the lambda.

In Sec. VI we derived the extreme ways of treating nonlocalities and mentioned that in coordinate space nonlocalities can be partially treated by replacing momenta by gradients. While the momentum space integrals in Eq. (29) treat nonlocalities exactly, the local approximations in Sec. VI freeze the operator at some constant proton momentum and, therefore, ignore nonlocal effects entirely. In Fig. 12 we compare the nonlocal calculation with the frozen proton approximation ($\mathbf{p}=0$) calculated in a relativistic formalism. Large differences are revealed for the high-spin transitions as well as the states that have lower cross sections. Therefore, when performing a relativistic calculation, it is important to include nonlocalities properly. On the other hand, nonlocal effects are small in the nonrelativistic calculation. Figure 13 shows a difference of about 10% for the high-spin states while the effects are more significant for lower spin states. Again, this result is subject to the elementary operator used since when using Thom's model for the elementary process the effect of nonlocalities in the nonrelativistic calculation can be as large as 50%. A large value of $g_{K\Lambda N}$ seems to suppress relativistic effects and nonlocal effects.

The results show in Figs. 12 and 13 were obtained using plane waves for the kaon, so that all the nonlocalities are due to Fermi motion. Figure 14 shows angular distributions comparing local and nonlocal DWIA calculations with the respective PWIA calculations performed in

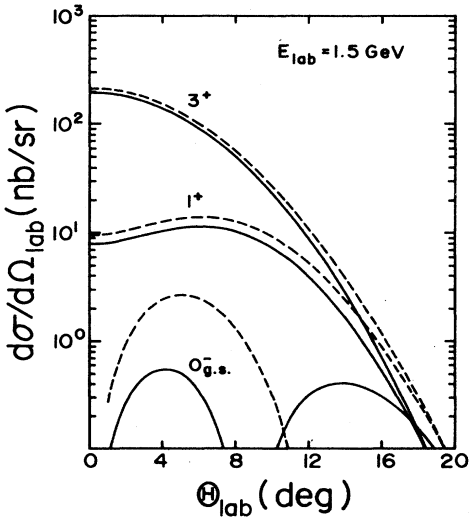

FIG. 13. Same as Fig. 12 but calculated in the nonrelativistic impulse approximation.

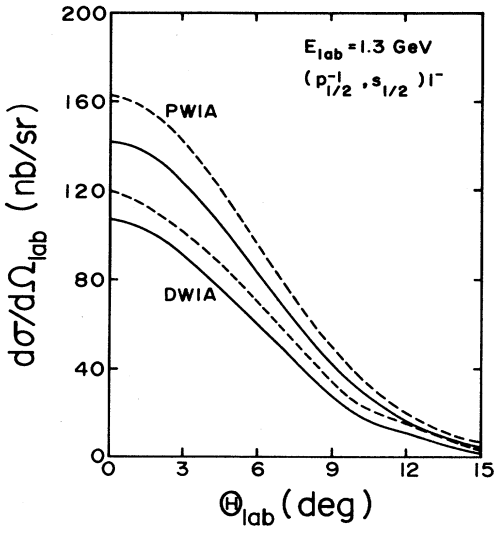

FIG. 14. Angular distributions showing the effect of distortion on the nonlocal (solid curves) and local (dashed curves) calculations.

a nonrelativistic framework. The difference of the two solid lines as compared to the difference between the two dashed lines changes very little indicating that the nonlocal effects arising from the smearing of the kaon momentum by the optical potential are minimal. This comes as no surprise since the kaon optical potential has such a simple form and is dominated by s-wave scattering which involves no gradients. This is to be contrasted with pion photoproduction where the nonlocal effects generated by the highly complex and stronger pion optical potential significantly alter the angular distributions.[15]

VIII. CONCLUSIONS

As the results presented in the previous sections show, the theoretical and calculational underpinnings of the investigation of hypernuclear states through kaon photoproduction are in place. A number of conclusions about various commonly made approximations follow from our investigations, but these conclusions are sensitive to the basic production operator as shown in Fig. 6. In fact, the largest uncertainties lie with the basic operator and this should be kept in mind since different basic operators affect the size of the other effects. In carrying out the remainder of our studies, we have used the best fit[13] available to photoproduction and electroproduction data which is AW IV as given in Table III. This fit has the advantage that the primary coupling constant is in rough agreement with that obtained from hadronic processes. While this gives us some confidence in our results, it is of crucial importance that additional photoproduction experiments from the proton be performed for photon energies from threshold up to about 2 GeV to confirm the basic operator.

Using the AW IV coupling constants and associated resonances, we showed the sensitivity of kaon photoproduction from ^{16}O to the use of a relativistic description of the bound baryons (the proton and the lambda). Unlike our previous results[12] using the operator fitted only to photodata which produced coupling constants in disagreement with hadronic analyses, we do not find tremendous relativistic effects on the larger cross sections. The effects are on the order of 30% although much larger effects show up in lower spin transitions and at larger momentum transfer. Again, we make the point that whether or not relativistic treatment of the bound baryons is important cannot be addressed without discussion of the operator in question.

We have also examined the contributions of nonlocalities arising from Fermi motion and the basic operator for the cases of both relativistic and nonrelativistic descriptions of the baryon wave functions. For high-spin transitions, which always have the largest cross sections within a cluster of almost degenerate states, we find that nonlocalities produce changes in the cross section of about 20% for the nonrelativistic baryon wave functions, while producing considerably larger effects for relativistic wave functions. A full relativistic calculation must include nonlocalities properly, while a nonrelativistic calculation makes a smaller error by using a local approximation. Furthermore, unlike the case of pion photoproduction, the inclusion of the kaon optical potential does not significantly increase the nonlocal contributions.

We also showed in Fig. 11 that retention of only the $\sigma\cdot\epsilon$ term in the production operator leads to appreciable variation in the cross section of the high-spin states only away from 0°. As usual, considerably larger effects are found in the lower spin transitions. Thus previous calculations of kaon photoproduction or electroproduction from nuclei with only this term and a frozen proton ($\mathbf{p}=0$) should be taken as preliminary away from 0°.

Finally, we note that the cross sections leading to the high-spin states are sufficiently large that 100% duty cycle linacs should be able to study them with either tagged photons or the use of virtual photon spectra near the end point.[41] Photon energies from theshold up to 2 GeV have been considered except one should keep in mind that the elementary operators were only fitted to data up to 1.4 GeV so that higher energy experiments from nuclei have even greater uncertainties in the elementary operator. For the first round of experiments, the energy range from 1 GeV up to 1.4 GeV would seem most appropriate. While we have carried out our investigations assuming ^{16}O is the target nucleus, our code can include all effects for any p-shell nucleus and can be easily extended to all nuclei. At the present time we need experimental data.

This work was supported in part by the U.S. Department of Energy Grant DE-FG02-87ER40370 and the Deutsche Forschungsgemeinschaft (SFB 201).

*Present address: Institut für Kernphysik, Johannes-Gutenberg-Universität Mainz, D-6500 Mainz, FRG.
[1]A. Gal, Adv. Nucl. Phys. **8**, 1 (1975).
[2]R. H. Dalitz, Nucl. Phys. **A354**, 101c (1981).
[3]C. B. Dover, Nucl. Phys. **A374**, 359c (1982).
[4]Proceedings of the International Symposium on Hypernuclear and Kaon Physics, Brookhaven National Laboratory, Upton, NY, 1985 [Nucl. Phys. **A450**, (1986)].
[5]C. B. Dover and G. E. Walker, Phys. Rev. C **89**, 1 (1982).
[6]S. R. Cotanch and S. S. Hsiao, Nucl. Phys. **A450**, 419c (1986), and references contained therein.
[7]A. M. Bernstein, T. W. Donnelly, and G. E. Epstein, Nucl. Phys. **A358**, 195 (1981).
[8]A. S. Rosenthal *et al.*, Ann. Phys. (N.Y.) **184**, 33 (1988); A. S. Rosenthal, D. Halderson, and I. Tabakin, Phys. Lett. B **182**, 143 (1986).
[9]J. Cohen, Phys. Rev. C **32**, 543 (1985); Proceedings of the CEBAF Summer Workshop, CEBAF, Newport News, Virginia, 1986 (unpubished).
[10]W. Brückner *et al.*, Phys. Lett. **79B**, 157 (1978); R. Bertini *et al.*, Nucl. Phys. **A368**, 365 (1981).
[11]R. E. Chrien *et al.*, Nucl. Phys. **A478**, 705c (1988).
[12]C. Bennhold and L. E. Wright, *Intersections Between Particle and Nuclear Physics, Lake Louise, 1986,* Proceedings of the Second Conference on the Intersections of Particle and Nuclear Physics AIP Conf. Proc. No. 150, edited by Donald F. Geessaman (AIP, New York, 1986), Vol. 150, p. 914; Phys. Lett. B **191**, 11 (1987); Prog. Part. Nucl. Phys. **20**, 377 (1988).
[13]R. A. Adelseck and L. E. Wright, Phys. Rev. C **38**, 1965 (1988).
[14]R. A. Adelseck, C. Bennhold, and L. E. Wright, Phys. Rev. C **32**, 1681 (1985).
[15]L. Tiator and L. E. Wright, Phys. Rev. C **30**, 989 (1984).
[16]B. C. Clark *et al.*, Phys. Rev. Lett. **50**, 644 (1983).
[17]L. D. Miller and A. E. S. Green, Phys. Rev. C **5**, 241 (1972).
[18]C. J. Horowitz and B. D. Serot, Nucl. Phys. **A368**, 503 (1981); **A399**, 529 (1983).
[19]L. D. Miller, Phys. Rev. Lett. **51**, 1733 (1983).
[20]J. D. Walecka, Ann. Phys. (N.Y.) **83**, 491 (1974).
[21]J. A. Carr, H. McManus, and K. Stricker-Bauer, Phys. Rev. C **25**, 952 (1982).
[22]B. R. Martin, Nucl. Phys. **B94**, 413 (1975).
[23]J. D. Bjorken and S. D. Drell, *Relativistic Quantum Mechanics* (McGraw-Hill, New York, 1964).
[24]T. W. Donnelly and W. C. Haxton, At. Data Nucl. Data Tables **23**, 103 (1979).
[25]S. Cohen and D. Kurath, Nucl. Phys. **73**, 1 (1965).
[26]A. Gal, J. M. Soper, and R. H. Dalitz, Ann. Phys. (N.Y.) **63**, 53 (1971); **72**, 445 (1972); **113**, 79 (1978); D. Halderson *et al.*, Phys. Rev. Lett. **57**, 1117 (1986).
[27]R. L. Huffman *et al.*, Phys. Rev. C **35**, 1 (1987).
[28]J. Cohen, M. W. Price, and G. E. Walker, Phys. Lett. B **188**, 393 (1987).
[29]J. M. Eisenberg and D. S. Koltun, *Theory of Meson Interactions with Nuclei* (Wiley, New York, 1980).
[30]L. Tiator, A. K. Rej, and D. Drechsel, Nucl. Phys. **A333**, 343 (1980).
[31]C. Bennhold, Ph.D. dissertation, Ohio University, 1987 (unpublished).
[32]I. Blomqvist and J. M. Laget, Nucl. Phys. **A280**, 405 (1977).
[33]S. Mehrotra and L. E. Wright, Nucl. Phys. **A362**, 461 (1981).
[34]R. Brockmann and W. Weise, Nucl. Phys. **A355**, 365 (1981).
[35]R. Brockmann, Phys. Rev. C **18**, 1510 (1978).
[36]C. Bennhold and L. E. Wright, Phys. Rev. C **36**, 438 (1987).
[37]J. Cohen, Phys. Rev. C **37**, 187 (1988).
[38]H. Thom, Phys. Rev. **151**, 1322 (1966).
[39]H. Tanabe, M. Kohno, and C. Bennhold, Mainz University Report (1988).
[40]J. V. Noble and R. R. Whitney, Conference on New Horizons in Electromagnetic Physics, (University of Virginia, Charlottesville, 1982) (unpublished).
[41]L. Tiator and L. E. Wright, Nucl. Phys. **A379**, 407 (1982).